Chinese Chemical Letters 31 (2020) 177–180

Contents lists available at ScienceDirect

Chinese Chemical Letters

journal homepage: www.elsevier.com/locate/cclet

Communication

3DRGO-$NiFe_2O_4$/NiO nanoparticles for fast and simple detection of organophosphorus pesticides

Zhenni Wei[a], Huiqing Li[a], Jing Wu[a], Yalei Dong[c], Hongyi Zhang[b], Hongli Chen[a], Cuiling Ren[a,*]

[a] State Key Laboratory of Applied Organic Chemistry, Key Laboratory of Nonferrous Metal Chemistry and Resources Utilization of Gansu Province, College of Chemistry and Chemical Engineering, Lanzhou University, Lanzhou 730000, China
[b] College of Chemistry and Environmental Science, Hebei University, Baoding 071002, China
[c] National Institutes for Food and Drug Control, Beijing 100050, China

ARTICLE INFO

Article history:
Received 2 March 2019
Received in revised form 14 May 2019
Accepted 16 May 2019
Available online 17 May 2019

Keywords:
3DRGO-$NiFe_2O_4$/NiO nanoparticles
Peroxidase-like activity
Organophosphorus pesticides (OPs)
Test paper
Smartphone

ABSTRACT

The residues of organophosphorus pesticide (OPs) on fruits and vegetables pose a threat to human health, so it is very meaningful to explore simple and fast detect methods for OPs residual. In this work, nickel ferrite/nickel oxide nanoparticles co-loaded three-dimensional reduced graphene oxide (3DRGO-$NiFe_2O_4$/NiO NPs), as a new low cost nanocomposite, was prepared. Based on its high performance mimetic peroxidase activity, a colorimetric method for the detection of OPs has been developed. Dichlorvos was chosen as model compounds to evaluate the detection performance. The detection linear range for dichlorvos is from 50 μg/mL to 2.5×10^4 μg/mL with a detection limit of 10 μg/mL. Furthermore, a test paper can be developed based on the 3DRGO-$NiFe_2O_4$/NiO NPs for visual detection of dichlorvos, and the image information of the paper sensor can be converted into digital signal and quantitative detection by a smartphone. Notably, this method can also be used to detect dichlorvos in real samples, including vegetables and fruits. Thus, the developed naked assay holds great potential in simple, inexpensive and rapid detection of OPs in fruit and vegetable samples.

Organophosphorus (OP) agents are a kind of widely used chemical pesticide in agricultural production. The residual of organophosphorus agents on agricultural products, especially on fruits and vegetables, can pose a threat to human health [1,2]. So the detection of OPs residual is very meaningful for human health. In the past several decades, a number of analytical methods have been put forward to determine OPs residues, such as liquid chromatography coupled with mass spectrometry (LC–MS) [3], gas chromatography coupled with mass spectrometry (GC–MS) [4], electrochemical analysis [5], fluorescent bioprobes [6], surface-enhanced Raman spectroscopy [7] and so on [8–10]. These approaches exhibit high sensitivity and selectivity. However, most of these approaches are suffered from high cost, complicated instruments, professional experimental techniques as well as sample pretreatment skills. Therefore, simple, fast and low cost approaches are urgent for pesticide residues detection.

Test paper can provide simple and valuable platform for OPs detection, which can be developed by colorimetric sensor. Until now, some colorimetric probes have been developed for visual detection of OPs [11–19]. Among them, sensor based on catalytic coloration is simple and fast, which can meet the real-time and rapid detection purposes. MFe_2O_4 (M = Mg, Ni, Cu, Co, Zn) nanomaterials have gained much attention in catalytic coloration, due to their stable thermal and chemical properties as well as simple storage and separation [20]. However, ferrite materials tend to aggregate which are not good for their catalytic applications. In order to solve this problem, 3D graphene was chosen as catalytic supports because it could provide more active sites by facilitating the mass transfer and maximizing the accessibility to the catalyst surfaces [21,22]. Noble metal is often used in preparing 3D graphene loaded magnetic nanocomposites, which have better catalytic performance, while the relative high cost is unfavorable for their applications. So it is necessary to prepare common metal-loaded 3D graphene composite to obtain the same or better catalytic properties compared with noble metals.

Meanwhile, convenient data analysis is also necessary for fast detection. With the popularity of smartphones, it can be used as portable device for data analysis due to their strong processing power. It is meaningful if smartphones can be used in detecting OPs based on paper sensors.

* Corresponding author.
E-mail address: rencl@lzu.edu.cn (C. Ren).

https://doi.org/10.1016/j.cclet.2019.05.031
1001-8417/

In this work, in order to achieve simple, rapid and low cost detection of OPs, on the one hand, nickel ferrite/nickel oxide nanoparticles co-loaded three-dimensional reduced graphene oxide (3DRGO-$NiFe_2O_4$/NiO NPs) were prepared for the first time and applied as a catalytic coloration sensor for visualization detection of OPs in this work. The preparation procedure was illustrated by Scheme S1 (Supporting information). Afterwards, paper sensor based on 3DRGO-$NiFe_2O_4$/NiO NPs was developed. As shown in Scheme S2 (Supporting information), H_2O_2 can be produced by acetylcholinesterase (AChE), choline oxidase (ChOx) and acetylcholine chloride (AChCl), and then react with 3,3′,5,5′-tetramethylbenzidine (TMB) rapidly on the 3DRGO-$NiFe_2O_4$/NiO NPs based paper sensor, leading to obvious blue color. The enzyme activity of AChE can be inhibited by OPs, resulting in less amount generation of H_2O_2 and color change depression of 3DRGO-$NiFe_2O_4$/NiO NPs-based colorimetric assay. On the other hand, the data of the paper sensor was further processed by smartphones.

The composition and structure of the as-prepared nanomaterials was analyzed by XRD spectra (Fig. 1A). The broad diffraction peak at 15°-30° corresponds to the (002) plane of graphite [23,24]. The diffraction peaks of $NiFe_2O_4$ NPs located at 18.4°, 30.2°, 35.6°, 43.3°, 57.3° and 62.9° are in correlation with (111), (220), (311), (400), (511) and (440) plane, respectively (JCPDS Powder Diffraction File No. 86-2267). The diffraction peaks appeared at 37.0° and 43.2° are corresponding to (111) and (200) plane of NiO NPs, respectively (JCPDS Powder Diffraction File No. 47-1049). While the XRD pattern of 3DRGO-$NiFe_2O_4$/NiO NPs were similar with that of 3DRGO-$NiFe_2O_4$, which may be attributed to the low crystallinity of NiO NPs, this speculation can be approved by the XRD spectra of 3DRGO-NiO NPs. The loads of NiO NPs on the porous three-dimensional graphene were further proved by TEM. As shown in Fig. 1B, compared with three-dimensional graphene, there are some nanoparticles were anchored on the 3DRGO-$NiFe_2O_4$/NiO NPs with an average diameter of 8–11 nm (inset). Fig. 1C showed more clearly lattice fringes interval; 0.210 nm corresponds to the (200) crystalline planes of NiO NPs [25,26], 0.250 and 0.300 nm are in agreement with the (311) and (220) planes of $NiFe_2O_4$ NPs [27]. Accordingly, it can be speculated that $NiFe_2O_4$ and NiO nanoparticles were co-anchored on the 3D graphene layers.

FT-IR spectra were used to identify the surface groups of the as-prepared 3DRGO-$NiFe_2O_4$/NiO NPs. As can be seen in Fig. 1D, the absorption peaks at 400–700 cm^{-1} can be attributed to the stretching vibration of metal-oxide [28]. The absorbance band at 490 cm^{-1} was attributed to the characteristic stretching vibrations of Ni-O and the peak at 602 cm^{-1} is associated with Fe-O stretching vibrations [29]. The peak at 3425 cm^{-1} shows O—H stretching [30]. The peaks at 1728, 1381 and 1201 cm^{-1} are in accordance with C=O, C—O, and —OH of the —COOH groups [23]. Meanwhile, the asymmetric and symmetric stretching vibrations of C—H bonds were located at 2852 and 2925 cm^{-1}, respectively [30]. The composition and surface oxidation state of the nanoparticles were elaborated by XPS (Fig. S1 in Supporting information).

The catalytic colorimetric assay was developed by using TMB as chromogenic substrate. The catalytic performance of enzyme mimetic depends on the reactant dosage (H_2O_2, TMB, 3DRGO-$NiFe_2O_4$/NiO NPs), temperature and pH value (Fig. S2 in Supporting information). The optimal pH is 3.8 and this acidic condition may cause the iron ions leached out into the solution, so the time-dependent absorbance comparison between 3DRGO-$NiFe_2O_4$/NiO NPs and iron leaching solution was conducted (Fig. S3a in Supporting information). It can be seen that the catalytic performance of iron leaching solution was negligible when compared with that of the 3DRGO-$NiFe_2O_4$/NiO NPs, because the leach amount of iron ions at pH 3.8 was as low as 0.1 mg/L (Fig. S3b in Supporting information). This result illustrates the high catalytic properties of the 3DRGO-$NiFe_2O_4$/NiO NPs came from the prepared material instead of the leached iron ions, and pH 3.8 can be chosen as the optimum condition.

Under the optimum conditions ([H_2O_2] = 0.2 mmol/L, [TMB] = 0.167 mmol/L, [3DRGO-$NiFe_2O_4$/NiO NPs] = 0.026 mg/mL, pH 3.8, 45 °C) the typical H_2O_2 concentration – response curves was shown in Fig. 2A, the linear range for H_2O_2 was from 0.4 μmol/L to 18 μmol/L, with a detection limit (LODs) of 0.1 μmol/L (calculated based on the $3\delta/k$ rule (δ is the standard deviation and k represents the slope of calibration curve)). Compared with other graphene-based nanohybrids (Table S1 in Supporting information), the nanomaterials synthesized in this work exhibit comparative or even more excellent catalytic performance.

The catalytic performance of 3DRGO-$NiFe_2O_4$/NiO NPs was further evaluated by kinetic assay. A typical Michaelis-Menten curve was obtained for 3DRGO-$NiFe_2O_4$/NiO NPs with suitable concentrations of H_2O_2 (Fig. S4a in Supporting information) or TMB (Fig. S4b in Supporting information) by monitoring the absorbance variation at 652 nm within the first 5 min. The maximum initial velocity (V_m) and Michaelis-Menten constant (K_m) for 3DRGO-$NiFe_2O_4$/NiO NPs obtained from the Lineweaver-Burk plots were listed in Table S2 (Supporting information). It can be seen that the V_m and K_m for 3DRGO-$NiFe_2O_4$/NiO NPs towards TMB was 0.110 mmol/L and 6.65×10^{-8} mol L^{-1} s^{-1}, respectively, and the K_m value has the same order of magnitude with noble-metal doped nanocatalyst. The values of K_m and V_m for 3DRGO-$NiFe_2O_4$/NiO NPs

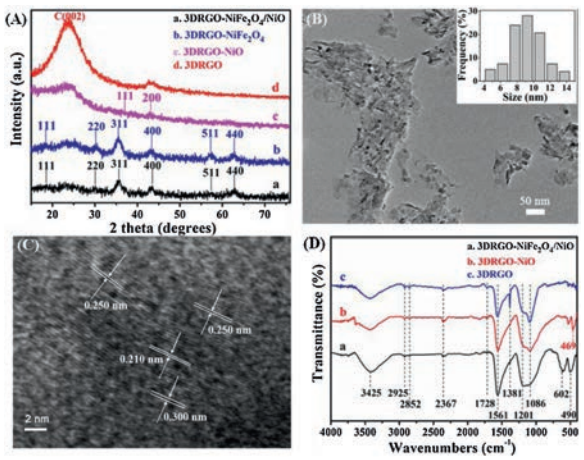

Fig. 1. (A) XRD patterns of 3DRGO-$NiFe_2O_4$/NiO NPs (curve a), 3DRGO-$NiFe_2O_4$ NPs (curve b), 3DRGO-NiO NPs (curve c), and 3DRGO (curve d). (B) TEM image (inset: size distribution diagram of the loaded nanoparticles) and (C) HRTEM image of 3DRGO-$NiFe_2O_4$/NiO NPs. (D) FT-IR spectra: 3DRGO-$NiFe_2O_4$/NiO NPs (curve a), 3DRGO-NiO NPs (curve b) as well as 3DRGO (curve c).

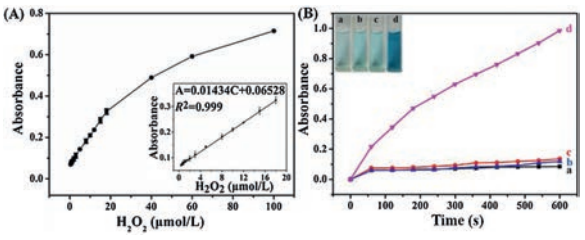

Fig. 2. (A) Dose-response curve for H_2O_2 detection. Inset shows respective linear calibration plots. The error bars represent the standard deviation of six measurements. (B) Time-dependent absorbance changes at 652 nm with different nanoparticles: 3DRGO (curve a), 3DRGO-NiO (curve b), 3DRGO-$NiFe_2O_4$ (curve c) and 3DRGO-$NiFe_2O_4$/NiO NPs (curve d). Inset: Images of TMB in the presence of H_2O_2 by the catalysis of 3DRGO (a), 3DRGO-NiO (b), 3DRGO-$NiFe_2O_4$ (c) and 3DRGO-$NiFe_2O_4$/NiO NPs (d).

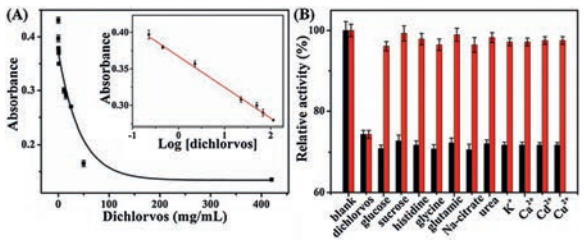

Fig. 3. (A) Dose-response curve for dichlorvos detection using 3DRGO-$NiFe_2O_4$/NiO NPs peroxidase mimetic-based colorimetric assay. Inset shows corresponding semilogarithmic plot of the data. (B) Selective and anti-interference assay by monitoring the absorbance variation at 652 nm with addition of different ions, amino acid and carbohydrate in the absence (black bars) and presence (red bars) of dichlorvos. The error bars represent the standard deviation of three measurements.

with H_2O_2 were 0.328 mmol/L and 11.74×10^{-8} mol L^{-1} s^{-1}, respectively.

Compared with the steady kinetic parameters of $NiFe_2O_4$, NiO and CeO_2/NiO nanoparticles (Table S2), 3DRGO-$NiFe_2O_4$/NiO NPs possesses lower K_m value with H_2O_2 [31–33]. The K_m value of 3DRGO-$NiFe_2O_4$/NiO with TMB was also less than that of 3DRGO-Fe_3O_4-Pd, Pd and Pt-pC_xN_{1-x} NPs [23,34,35]. These data demonstrated that the anchor of NiO NPs and $NiFe_2O_4$ NPs on 3DRGO sheets obviously improved their affinity toward H_2O_2 [36], thus it showed excellent catalytic activity even though there is no noble metal present. Meanwhile, three parallel lines of double-reciprocal plots conformed to ping-pong mechanism in Figs. S4c and d (Supporting information) [23,37].

Furthermore, as shown in Fig. 2B, 3DRGO-NiO NPs and 3DRGO-$NiFe_2O_4$ NPs showed very weak catalytic effect compared with that of 3DRGO-$NiFe_2O_4$/NiO NPs. It can be speculated that the excellent catalytic performance of the prepared 3DRGO-$NiFe_2O_4$/NiO NPs stem from the synergistic effect of the NiO NPs and $NiFe_2O_4$ NPs on the 3DRGO layer.

The mechanism of catalytic colorimetric assay might be ascribed to ·OH radical which generated from H_2O_2 catalyzed by 3DRGO-$NiFe_2O_4$/NiO NPs. In the present of ·OH, terephthalic acid can produce highly fluorescent 2-hydroxy terephthalic acid [38], so terephthalic acid was used as fluorescent sensor to test ·OH. As shown in Fig. S5 (Supporting information), the fluorescence intensity of the sensor gradually enhanced with the catalyst dosage increasing, and no fluorescent signal can be detected when no H_2O_2 was added. This result verifies the color change of the solution was stem from the oxidation of TMB caused by the OH radical.

Magnetization curve of 3DRGO-$NiFe_2O_4$/NiO NPs illustrated the magnetic nanoparticles are superparamagnetic with a magnetic saturation value of 6.05 emu/g (Fig. S6 in Supporting information), they could be separated easily from the mixture by a magnet (inset in Fig. S6 in Supporting information). This property endows this material can be reused and their catalytic effects retained 82.51% after recycled for ten times (Fig. S7 in Supporting information).

In order to evaluate the practical application of the prepared 3DRGO-$NiFe_2O_4$/NiO NPs in visual detection of OPs, dichlorvos was selected as a representative analyte. The enzyme inhibition reaction was carried out in appropriate conditions. Fig. S8 (Supporting information) showed the influence of temperature, pH, incubation time as well as the concentrations of AChCl and AChE on the detection performance of this assay. The best detection result was obtained when using 4 U/mL of AChE, 0.5 U/mL of ChOx and 5 mmol/L of AChCl reacted under pH of 3.8 at room temperature for 10 min. The dose-dependent response of dichlorvos and corresponding semilogarithmic plot were shown in Fig. 3A. Dichlorvos can be detected in the range of 50 μg/mL to 2.5×10^4 μg/mL with a detection limit of 10 μg/mL, which was almost equal to the maximum residue limit reported in the European Union Agriculture (0.01 mg/mL). [39]. Compared with the reported work (Table S3 in Supporting information), the colorimetric method in this work exhibits notable sensitivity with a wide linear range which could be owed to the highly catalytic effects of 3DRGO-$NiFe_2O_4$/NiO NPs.

Selective assay was evaluated to identify the detection ability of this colorimetric method for dichlorvos. 0.45 mmol/L of different ions (K^+, Ca^{2+}, Cd^{2+}, Cu^{2+} and sodium citrate), amino acid (histidine, glycine, glutamic) and carbohydrate (glucose and sucrose) were added in the absence of dichlorvos (black bars in Fig. 3B). Competition experiments were conducted by subsequently adding dichlorvos to each solution (red bars in Fig. 3B) [40]. The concentration of the interferents is 1000 times as high as that of the OPs. The results showed that this colorimetric method has good selectivity for OPs detection [39].

A test paper based on 3DRGO-$NiFe_2O_4$/NiO NPs for dichlorvos detection was developed. As shown in Fig. 4A, the color of the test paper was blue at first, the addition of dichlorvos make the blue color become lighter, and the depression degree is proportional to the concentration of dichlorvos (from 0 to 50 mg/mL). The color change can be distinguished by naked eyes, the quantitative analysis can be achieved by using smartphone. The image signal was converted into data saturation (S) and lightness (L) by APP acquired from the smartphone screen. To improve the detection sensitivity and repetition performance of this method, the ratio of S to L was selected as analysis signal. A linear relationship S/L = 0.43326–0.06319log[dichlorvos] (R^2 = 0.99, LOD of 10 μg/mL) was calculated by S/L and logarithm of dichlorvos concentration in Fig. 4B. According to the APP analysis, the detected pesticide was less than 10 μg/mL when the value of S/L was higher than 0.518. As a consequence, the convenient and fast APP method on the smartphone was successfully used in dichlorvos detection.

For the sake of application in real samples, the efficiency of the proposed colorimetric array in vegetables and fruits was further investigated. As shown in Table S4 (Supporting information), the recoveries of dichlorvos in these samples were in the range of 84.2%–112.0% with a relative standard deviation (RSD) of less than 1.9%, which indicated that this method can be applied in OPs residues detection in real samples.

To further verify the feasibility of the combination of paper sensor and APP in detecting dichlorvos residue in real samples, vegetables and fruits sprayed with a certain amount of dichlorvos before and after washing with water was tested by the paper sensor and the image results were processed by smartphone (Fig. 5 and Table 1). As a systemic pesticide, dichlorvos can enter the crop after field application. So the test paper developed by this work can be used

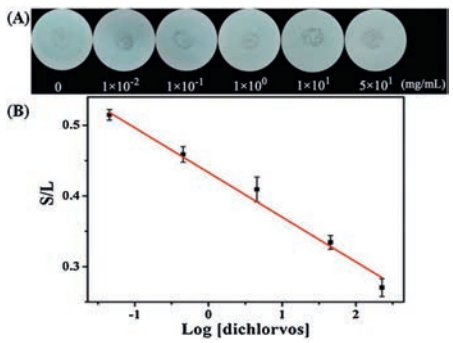

Fig. 4. (A) Photographs of 3DRGO-$NiFe_2O_4$/NiO NPs based paper sensor with different concentration of dichlorvos under sunlight and (B) linear relationship analyzed by smartphone APP.

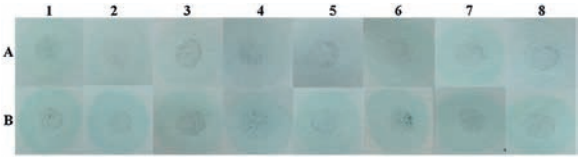

Fig. 5. Photographs of 3DRGO-$NiFe_2O_4$/NiO NPs based paper sensor for real samples before (A) and after (B) washing: 1. Chinese cabbage, 2. pepper, 3. eggplant, 4. cucumber, 5. tomato, 6. apple, 7. grape, 8. pear.

Table 1
S/L values of real samples sprayed with dichlorvos before (A) and after (B) washing.

Samples	1	2	3	4	5	6	7	8
A	0.319	0.330	0.307	0.340	0.339	0.334	0.418	0.346
B	0.475	0.523	0.371	0.502	0.480	0.529	0.450	0.498

1. Chinese cabbage, 2. pepper, 3. eggplant, 4. cucumber, 5. tomato, 6. apple, 7. grape, 8. pear.

to evaluate the cleaning efficiency of the residual dichlorvos on the surface of fruits and vegetables. According to the S/L value in Table 1, little amount of dichlorvos was left on the surface of pepper and apple after cleaning, but other samples need further washing.

In summary, nickel ferrite/nickel oxide nanoparticles-co-loaded three-dimensional reduced graphene oxide (3DRGO-$NiFe_2O_4$/NiO NPs) was prepared by a one-pot hydrothermal method, which showed intrinsic peroxidase-like activity and high affinity toward H_2O_2, so a colorimetric method based on mimetic peroxidase 3DRGO-$NiFe_2O_4$/NiO NPs for OPs detection has been developed. Dichlorvos was chosen as model compounds to evaluate the detection performance. The detection linear range for dichlorvos is from 50 μg/mL to 2.5×10^4 μg/mL with a LOD of 10 μg/mL. This method can also be used to detect dichlorvos in real samples, including fruits and vegetables. Furthermore, a test paper can be developed based on the 3DRGO-$NiFe_2O_4$/NiO NPs for visual detection of dichlorvos. Notably, the image information of the paper sensor can be converted into digital signal and quantitative detection by a smartphone. Thus, we provided a simple and inexpensive assay for rapid detection of dichlorvos, which has a great potential application for other OPs detection in environmental chemistry.

Acknowledgments

This work was financially supported by the National Natural Science Foundation of China (Nos. 21874061, 21207057, 21405159, 21505061) and the Fundamental Research Funds for the Central Universities (Nos. lzujbky-2016-43, lzujbky-2018-80).

Appendix A. Supplementary data

Supplementary material related to this article can be found, in the online version, at doi:https://doi.org/10.1016/j.cclet.2019.05.031.

References

[1] M.M. Liang, K.L. Fan, Y. Pan, et al., Anal. Chem. 85 (2013) 308–312.
[2] F. Nachon, X. Brazzolotto, M. Trovaslet, P. Masson, Chem. Biol. Interact. 206 (2013) 536–544.
[3] H.G.J. Mol, R.C.J. van Dam, O.M. Steijger, J. Chromatogr. A 1015 (2003) 119–127.
[4] J. Blesa, J.M. Soriano, J.C. Moltó, R. Marı'n, J. Mañes, J. Chromatogr. A 1011 (2003) 49–54.
[5] R. Xue, T.F. Kang, L.P. Lu, S.Y. Cheng, Anal. Lett. 46 (2013) 131–141.
[6] J. Fu, X. An, Y. Yao, Y. Guo, X. Sun, Sens. Actuators B-Chem. 287 (2019) 503–509.
[7] W. Fang, X.W. Zhang, Y. Chen, et al., Anal. Chem. 87 (2015) 9217–9224.
[8] W. Song, H.J. Zhang, Y.H. Liu, C.L. Ren, H.L. Chen, Chin. Chem. Lett. 28 (2017) 1675–1680.
[9] X. Gao, G.C. Tang, X.G. Su, Biosens. Bioelectron. 36 (2012) 75–80.
[10] X. Yan, H.X. Li, X.S. Han, X.G. Su, Biosens. Bioelectron. 74 (2015) 277–283.
[11] G. Santoni, J. de Sousa, E. de la Mora, et al., J. Med. Chem. 61 (2018) 7630–7639.
[12] T.L. Rosenberry, X. Brazzolotto, I.R. Macdonald, et al., Molecules 22 (2017) 2098.
[13] S.H. Qian, H. Lin, Anal. Chem. 87 (2015) 5395–5400.
[14] X.X. Hu, Y.T. Su, Y.W. Ma, et al., Chem. Commun. 51 (2015) 15118–15121.
[15] S. Palanisamy, S.M. Chen, R. Sarawathi, Sensor. Actuat. B -Chem. 166–167 (2012) 372–377.
[16] G. Rebollar Pérez, F. Lima Zambrano, G. Bairán, et al., Environ. Eng. Sci. 33 (2016) 951–961.
[17] E. Climent, M. Biyikal, K. Gawlitza, et al., Sensor. Actuat. B -Chem. 246 (2017) 1056–1065.
[18] Y. Li, Q.J. Luo, R. Hu, Z.B. Chen, P. Qiu, Chin. Chem. Lett. 29 (2018) 1845–1848.
[19] H.X. Zhang, R.B. Wei, C.Z. Chen, X.L. Tuo, X.G. Wang, Chin. Chem. Lett. 26 (2015) 39–42.
[20] L. Su, J. Feng, X. Zhou, et al., Anal. Chem. 84 (2012) 5753–5758.
[21] Z.S. Wu, S.B. Yang, Y. Sun, et al., J. Am. Chem. Soc. 134 (2012) 9082–9085.
[22] B.C. Qiu, Y.X. Deng, M.M. Du, M.Y. Xing, J.L. Zhang, Sci. Rep. 6 (2016) 29099.
[23] X.J. Zheng, Q. Zhu, H.Q. Song, et al., ACS Appl. Mater. Interfaces 7 (2015) 3480–3491.
[24] X.H. Zhao, X. Liu, RSC Adv. 5 (2015) 79548–79555.
[25] C. Chang, L. Zhang, C. Hsu, X.F. Chuah, S. Lu, ACS Appl. Mater. Interfaces 10 (2018) 417–426.
[26] J.S. Mu, X. Zhao, J. Li, E.C. Yang, X.J. Zhao, J. Mater. Chem. B 4 (2016) 5217–5221.
[27] M. Fu, Q.Z. Jiao, Y. Zhao, J. Mater. Chem. A 1 (2013) 5577–5586.
[28] M. Mouallem-Bahout, S. Bertrand, O. Peña, J. Solid State Chem. 178 (2005) 1080–1086.
[29] K.C. Babu Naidu, W. Madhuri, Mater. Sci. 40 (2017) 417–425.
[30] S.Q. Liu, B. Xiao, L.R. Feng, et al., Carbon 64 (2013) 197–206.
[31] L. Su, W.J. Qin, H.G. Zhang, et al., Biosens. Bioelectron. 63 (2015) 384–391.
[32] C. Ray, S. Dutta, S. Sarkar, et al., J. Mater. Chem. B 2 (2014) 6097–6105.
[33] J.S. Mu, X. Zhao, J. Li, E.C. Yang, X.J. Zhao, Mater. Sci. Eng. C-Mater. 74 (2017) 434–442.
[34] J.M. Lan, W.M. Xu, Q.P. Wan, et al., Anal. Chim. Acta 825 (2014) 63–68.
[35] X.M. Lei, T.T. Li, Y.P. Zuo, et al., Electrochim. Acta 209 (2016) 661–670.
[36] Y.P. Liu, F.Q. Yu, Nanotechnology 22 (2011) 145704.
[37] F.F. Liu, J. He, M.L. Zeng, et al., J. Nanopart. Res. 18 (2016) 106.
[38] A. Fujishima, T.N. Rao, D.A. Tryk, J. Photochem. Photobiol. C 1 (2000) 1–21.
[39] J.Y. Hou, Z.B. Tian, H.Z. Xie, Q.Y. Tian, S.Y. Ai, Sensor. Actuat. B -Chem. 232 (2016) 477–483.
[40] R. Zhang, N. Li, J.Y. Sun, F. Gao, J. Agric. Food. Chem. 63 (2015) 8947–8954.